

Effect of laser surface melting on corrosion behaviour of AZ91D Mg alloy in simulated-modified body fluid

Y. C. Guan · Wei Zhou · H. Y. Zheng

Received: 23 September 2008 / Accepted: 2 February 2009 / Published online: 19 February 2009
© Springer Science+Business Media B.V. 2009

Abstract High corrosion rate in physiological environment of the body is the major drawback of magnesium alloys for their successful applications as biodegradable orthopaedic implants. In the present study, corrosion behaviour of AZ91D magnesium alloy after laser surface melting (LSM) was studied in modified-simulated body fluid at 37 °C. The improved corrosion resistance of AZ91D alloy using LSM was found to depend on the solidification microstructure in the laser-melted zone. The general and pitting corrosion resistance of laser-treated surface was significantly enhanced due to the refined continuous network of β -Mg₁₇Al₁₂ phases and the increased Al concentration in the laser-melted zone.

Keywords Magnesium alloy · Laser surface melting · Biodegradation · Corrosion

1 Introduction

In recent years, research and development work on magnesium and magnesium-based alloys for bio-implant applications has increased significantly [1–3]. Compared with traditional implants such as stainless steels, titanium alloys and cobalt–chromium-based alloys, magnesium

alloys are much more attractive mainly due to their degradation behaviour in the human body [1]. Unfortunately, magnesium alloy implants corrode very quickly at pH level of 7.4–7.6 and in the high-chloride environment of the physiological system. Consequently, the implant will lose its mechanical integrity before the tissues sufficiently heal [1–3]. Therefore, improving corrosion resistance is an important issue for the application of magnesium alloys as biodegradable load-bearing implants.

AZ91D is one of the most widely used Mg alloys. In this alloy, β -Mg₁₇Al₁₂ intermetallic phase normally helps to improve the corrosion resistance [4, 5], but the effectiveness of this phase in improving the corrosion resistance depends on its amount and distribution in the α -Mg matrix [6–9]. A fine and homogeneous β -Mg₁₇Al₁₂ phase provides an effective anticorrosion barrier; however, the presence of coarse and nonhomogeneously distributed β -Mg₁₇Al₁₂ phase could deteriorate the corrosion performance as it can act as a galvanic cathode [6]. The beneficial effect of β -Mg₁₇Al₁₂ phase on the corrosion resistance may be enhanced significantly using laser surface melting due to the refinement of microstructure and increase of Al concentration [10–12]. The objective of this research was to study how laser surface melting could be explored to improve corrosion resistance of AZ91D alloy in modified-simulated body fluid (m-SBF).

2 Materials and methods

The material studied was AZ91D Mg alloy with the following chemical composition (wt.%): Al 8.97, Zn 0.78, Mn 0.31, Si 0.023, Cu 0.002, Ni 0.0005 and Mg balance. The specimens were extracted from the ingot, ground with progressively finer SiC paper (180, 400, 800, 1,200, 2,400

Y. C. Guan · W. Zhou (✉)
Precision Engineering and Nanotechnology Centre, School
of Mechanical and Aerospace Engineering, Nanyang
Technological University, 50 Nanyang Avenue,
Singapore 639798, Singapore
e-mail: wzhou@cantab.net

W. Zhou · H. Y. Zheng
Singapore Institute of Manufacturing Technology, 71 Nanyang
Drive, Singapore 638075, Singapore

Table 1 Main processing parameters used for laser surface melting of AZ91D Mg alloy

Specimen ID	Power density (W cm ⁻²)	Scanning speed (mm s ⁻¹)	Frequency (Hz)	Overlap (%)	Pulse duration (ms)
A	3.82×10^4	5	100	50	1.0
B	3.82×10^4	10	100	50	1.0
C	3.82×10^4	20	100	50	1.0
D	3.82×10^4	30	100	50	1.0

and 4,000 grit), cleaned with alcohol and then irradiated with Lumonics JK704 Nd:YAG laser system. The laser processing parameters are given in Table 1. Microstructural features of the specimens were studied using a JEOL 5600LV SEM equipped with an energy-dispersive X-ray spectrometer (EDX). The EDX measurements provided information on the chemical composition. Identification of phases formed in the as-received alloy and the laser-melted layer was performed using X-ray diffractometer (Philips PW1710 series).

In vitro corrosion test was carried out in modified-simulated body fluid (m-SBF) maintained at a temperature of 37 °C. The composition of m-SBF is given in Table 2 [3, 13]. The solution was buffered with 2-(4-(2-hydroxyethyl)-1-piperazinyl) ethanesulfonic acid (HEPES) at a physiological pH of 7.4, and it had optimum ion concentration for in vitro bioactivity assessment of artificial materials and biomimetic production of bone-like apatite [13].

Corrosion rates of the as-received and laser-treated AZ91D specimens were measured in the m-SBF using constant immersion test for five different intervals of time (2 h, 1 day, 3 days, 7 days and 14 days). Before each test, the specimen was ground on progressively finer grades of emery paper (up to 4,000) and then weighed. Cleaning of the specimen was carried out at the end of the immersion test by dipping it into a solution of 15% CrO₃ + 1% AgCrO₄ in 100 mL water at boiling temperature [4]. An acetone washing followed this. The weight loss was measured after each experiment and the corrosion rate was

Table 2 Chemical composition of m-SBF [3, 13]

Reagents	Amount
NaCl (g)	5.403
NaHCO ₃ (g)	0.504
Na ₂ CO ₃ (g)	0.426
KCl (g)	0.225
K ₂ HPO ₄ · 3H ₂ O (g)	0.23
MgCl ₂ · 6H ₂ O (g)	0.311
CaCl ₂ (g)	0.293
Na ₂ SO ₄ (g)	0.072
1 M NaOH (mL)	15
0.2 M NaOH (mL)	100
HEPES (mL)	17.892

HEPES 2-(4-(2-hydroxyethyl)-1-piperazinyl) ethanesulfonic acid

calculated from the weight loss and specimen surface area in mg cm⁻² week⁻¹.

The electrochemical corrosion behaviour of the as-received and laser-treated AZ91D specimens was studied using potentiostat/galvanostat corrosion measurement system (EG&G model 263A). The specimens were ground prior to the experiment, washed with distilled water and then ultrasonically cleaned in acetone. A potentiodynamic polarisation test was carried out in a Model K0235 Flat Cell Kit using AgCl/Ag electrode as the reference electrode and the specimen as the working electrode. About 1 cm² surface area of the specimen was exposed to 150 mL m-SBF at 37 °C. A polarization scan was carried out towards more noble values at a rate of 0.8 mV s⁻¹, after allowing the steady-state potential to develop.

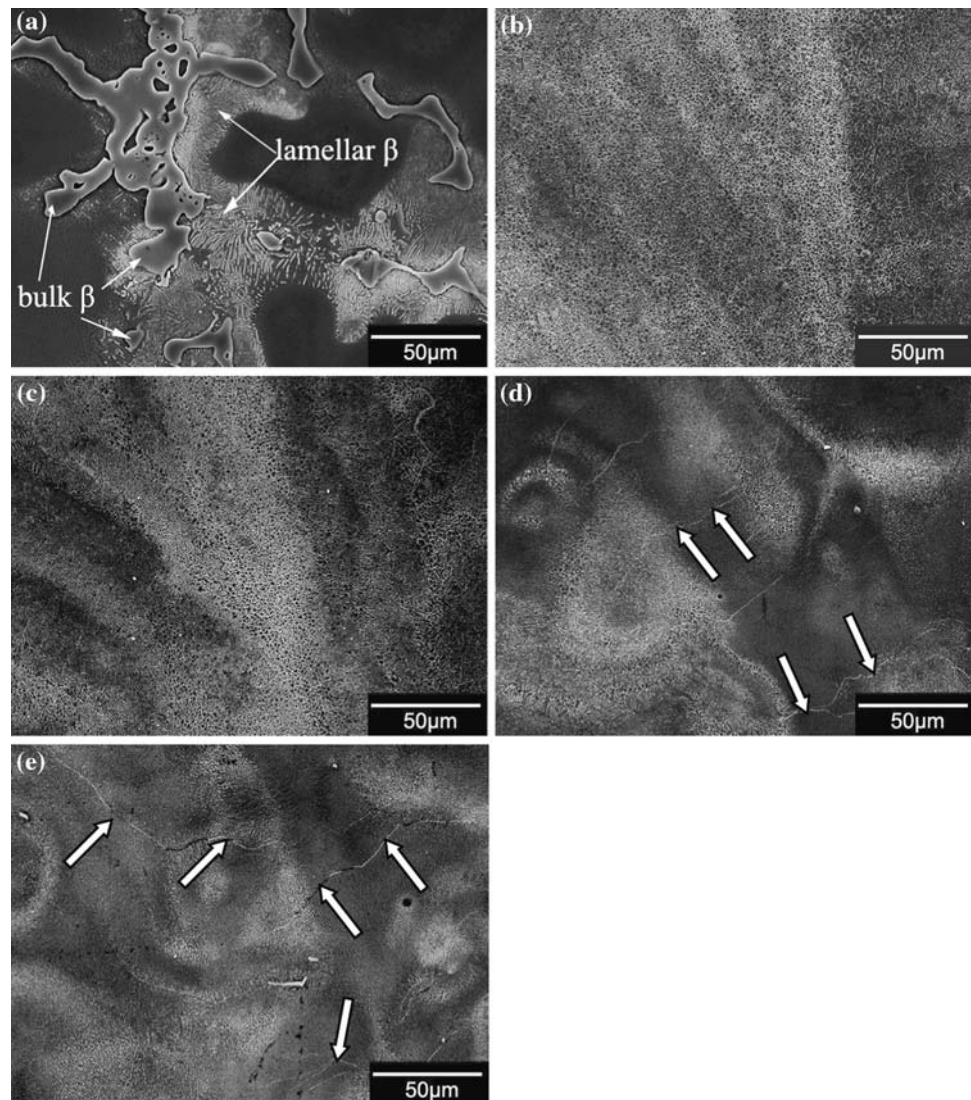
3 Results and discussion

3.1 Microstructures

Microstructure of the as-received AZ91D alloy mainly consisted of α -Mg phase as the alloy matrix, bulk β -Mg₁₇Al₁₂ intermetallic phase and lamellar β -Mg₁₇Al₁₂ structure, as shown in Fig. 1a. The β -Mg₁₇Al₁₂ phase in the as-received alloy was found to be distributed nonuniformly in the α -Mg matrix.

Microstructure of the AZ91D alloy was changed significantly by the laser surface melting process. In the laser-treated surfaces, almost all the β -Mg₁₇Al₁₂ intermetallics were refined and distributed uniformly, and the solidification microstructure was mainly cellular/dendritic structure with the continuous network of β -Mg₁₇Al₁₂ phase precipitated interdendritically (Figs. 1b–e, 2). Moreover, coarse dendritic structures were found to form along the overlapped regions due to the remelting process [10–12]. Compared with other LSM specimens, larger remelted regions were found in specimen A due to its slowest laser scanning rate, as shown in Figs. 1b and 2a. Furthermore, with the scanning rates increasing, less remelted regions and small cracks were found in the laser-melted zones in specimens C and D due to higher internal stress during the very fast cooling process [14, 15] (Figs. 1d, e, 2c, d). Figure 3 shows typical X-ray diffraction patterns of AZ91D alloy before and after laser treatment. The patterns

Fig. 1 Scanning electron micrographs showing original surfaces of AZ91D alloy before corrosion tests **a** as-received alloy, **b** specimen A, **c** specimen B, **d** specimen C (with cracks arrowed) and **e** specimen D (with cracks arrowed)



confirm the presence of α -Mg phase and β -Mg₁₇Al₁₂ intermetallic phase in both as-received and laser-treated microstructures.

It is worthwhile to note that magnesium alloys have high thermal expansion coefficient ($16.1 \times 10^{-6} \text{ K}^{-1}$ between 20 °C and 400 °C) [16], so the tensile stress is expected to be high during thermal contraction of the laser-melted zone. Zhou et al. observed thermal-stress-induced cracking in AZ91D alloy after surface melting using tungsten inert gas [17]. In the current study, cracking was observed in specimens C and D but not in specimens A or B. As laser scanning rate increased from 5 and 10 mm s⁻¹ for specimens A and B to 20 and 30 mm s⁻¹ for specimens C and D (Table 1), the laser heating time decreased considerably and thus the temperature gradients in the melted zone increased significantly, leading to larger thermal tensile stresses in specimens C and D than in specimens A and B. This explains why specimens C and D are more susceptible

to cracking. Gas porosity is a very common structural defect formed during die-casting of magnesium alloys [18], but no such defect was observed in any of the specimens (Figs. 1, 2).

Quantitative analyses of chemical compositions in the melted zone were carried out using EDX at around 30 different spots for each laser-treated specimen. The average Al concentration in the laser-treated layer was calculated as 11.7 wt.%, which was higher than the Al concentration of 9.0 wt.% in the as-received material. The increased average Al concentration in the melted zone is likely due to more Mg evaporation during the laser process [14, 19, 20].

3.2 Effect of laser surface melting on corrosion rates

Variation of corrosion rate with immersion time for the as-received and laser-treated specimens is presented in Fig. 4. Specimens A and B for varying immersion time all gave

Fig. 2 High-magnification scanning electron micrographs showing microstructures of AZ91D alloy after laser surface melting **a** specimen A, **b** specimen B, **c** specimen C (with cracks) and **d** specimen D (with cracks)

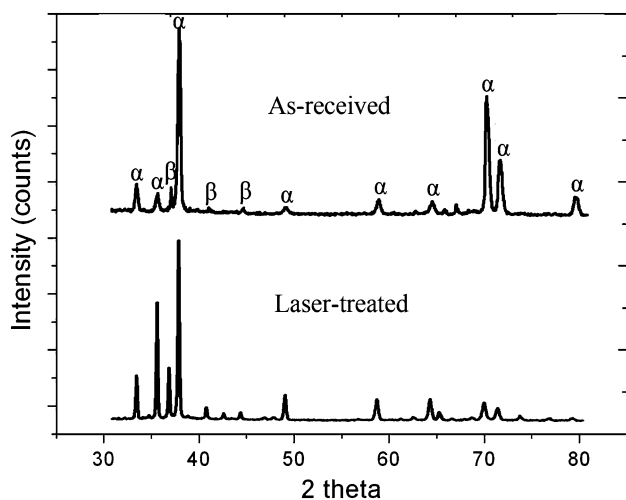
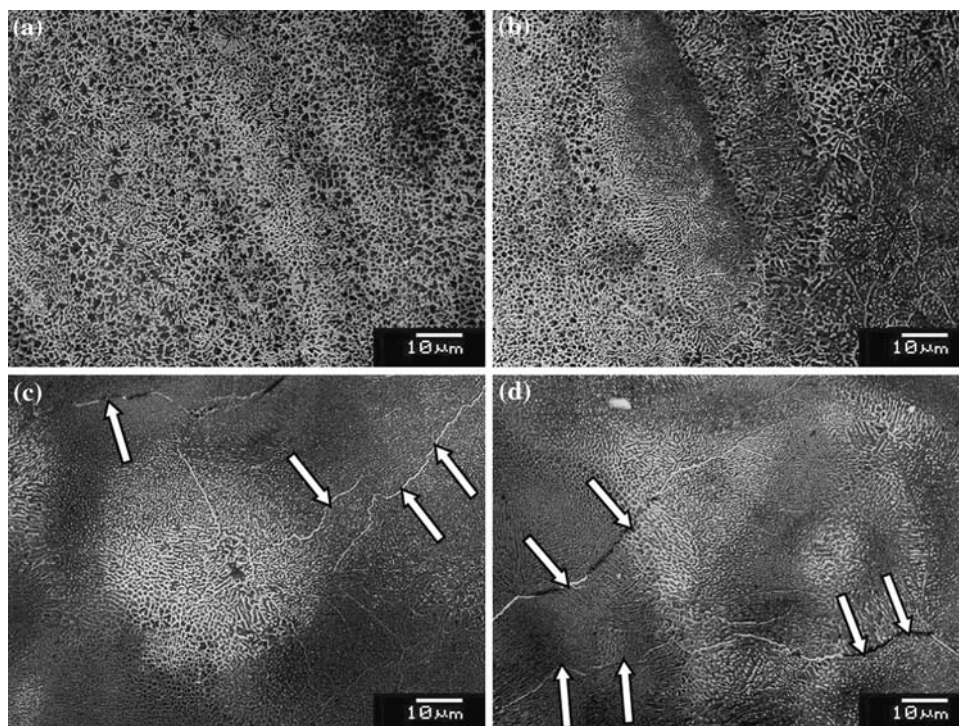


Fig. 3 Typical X-Ray diffraction patterns of AZ91D Mg alloy before and after laser irradiation

lower corrosion rates than the as-received microstructure due to the refined β -Mg₁₇Al₁₂ phase. Moreover, specimen B showed the lowest corrosion rate among all the LSM specimens. The corrosion rate of specimen A was higher than that of specimen B due to the coarser dendritic structures in the overlapped regions, which were more likely to be corroded and decreased the overall corrosion resistance [10–12]. Moreover, corrosion rates of specimens C and D are shown in Fig. 4 to increase with immersion time due to the presence of small cracks in the melted zones (see Figs. 1d, e, 2c, d).

The typical surface features for corrosion initiation and growth stages of specimens A and B after different times of exposure are shown in Figs. 5 and 6. Corrosion started initially at localized sites of the overlapped regions in specimen A and the localized attack invaded the entire surface with continued exposure. After 2 weeks of immersion in m-SBF, the overlapped regions in specimen A were highly damaged, as shown in Fig. 5. For specimen B, corrosion in the form of pitting initiated preferentially along the grain boundaries, but pits were clearly observed to be present within α -Mg grains after exposure of 3 days. Corrosion was found to propagate with increasing exposure time but the degree of corrosion was lower in specimen B (Fig. 6) than in specimen A (Fig. 5). The results are consistent with the assessment that specimen B gives the best corrosion resistance.

In order to understand the effect of microstructural features on corrosion mechanism in greater detail, the corroded surfaces of 2 h and 2 weeks exposures were carefully analyzed under SEM. Selected SEM micrographs for corroded surfaces of as-received specimen and laser-treated specimens A, B and C are shown in Figs. 7 and 8.

In the initial 2 h exposure, corrosion of the as-received microstructure occurred preferentially in α -Mg matrix and the eutectic area, and intergranular and pitting corrosion was found along the original β -Mg₁₇Al₁₂ phase (Fig. 7a). For LSM microstructures A, B and C, deep corrosion was observed along the overlapped regions while some localized corrosion was found within the matrix (Fig. 7b–d). Coarse dendritic structures in specimen A and small cracks

Fig. 4 Corrosion rate for as-received and laser-treated surface in m-SBF **a** after 2 h and **b** after 2 weeks

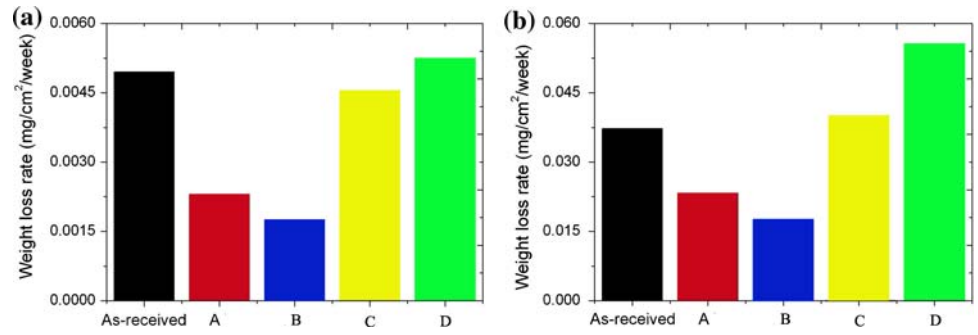


Fig. 5 Corrosion rate for specimen A in m-SBF as a function of exposure time

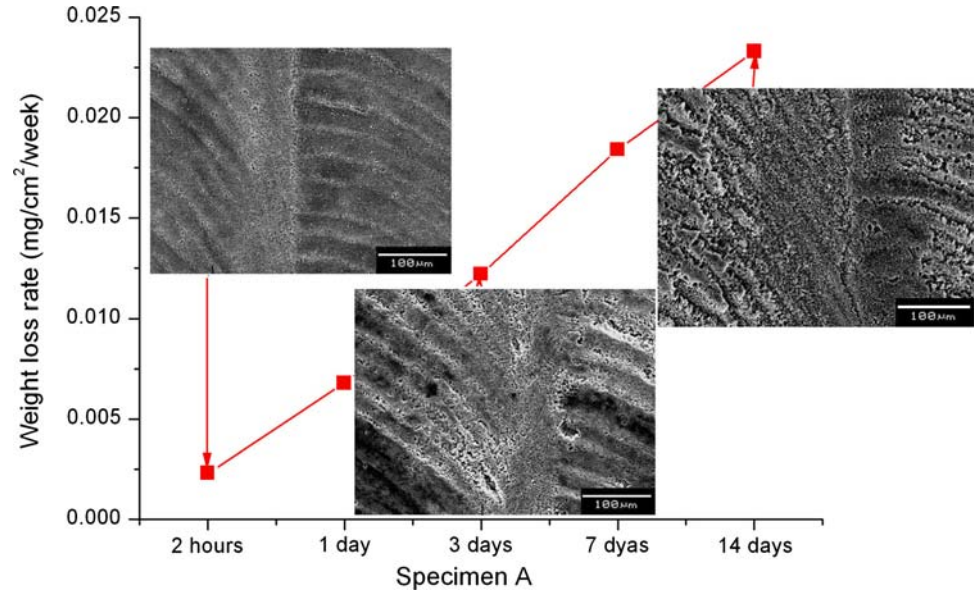


Fig. 6 Corrosion rate for specimen B in m-SBF as a function of exposure time

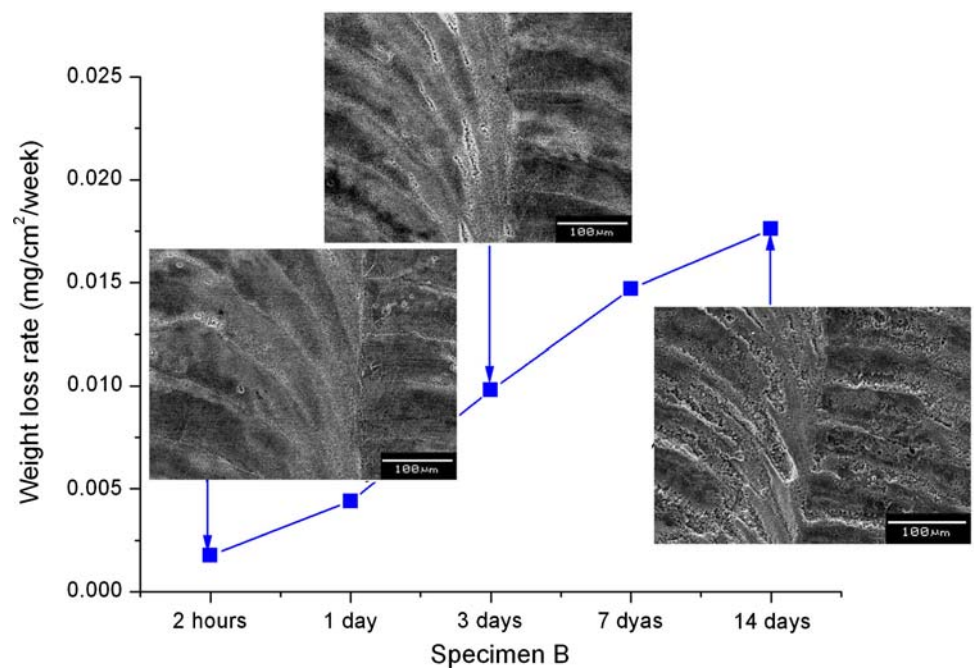


Fig. 7 Scanning electron micrographs showing corroded surfaces of **a** as-received alloy, **b** specimen A, **c** specimen B and **d** specimen C in m-SBF after 2 h exposure

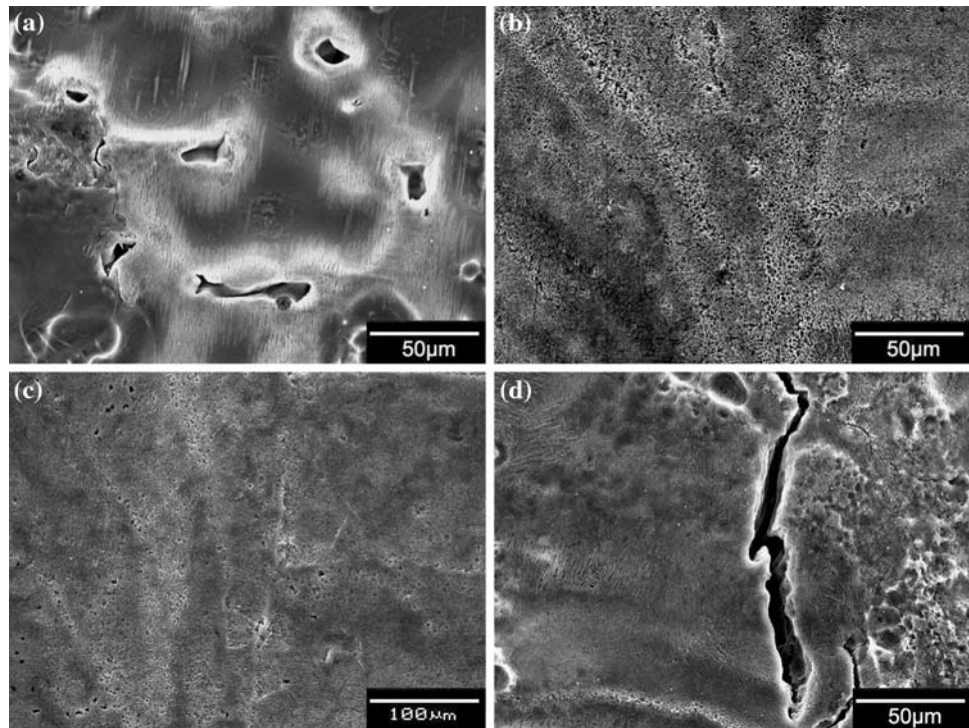
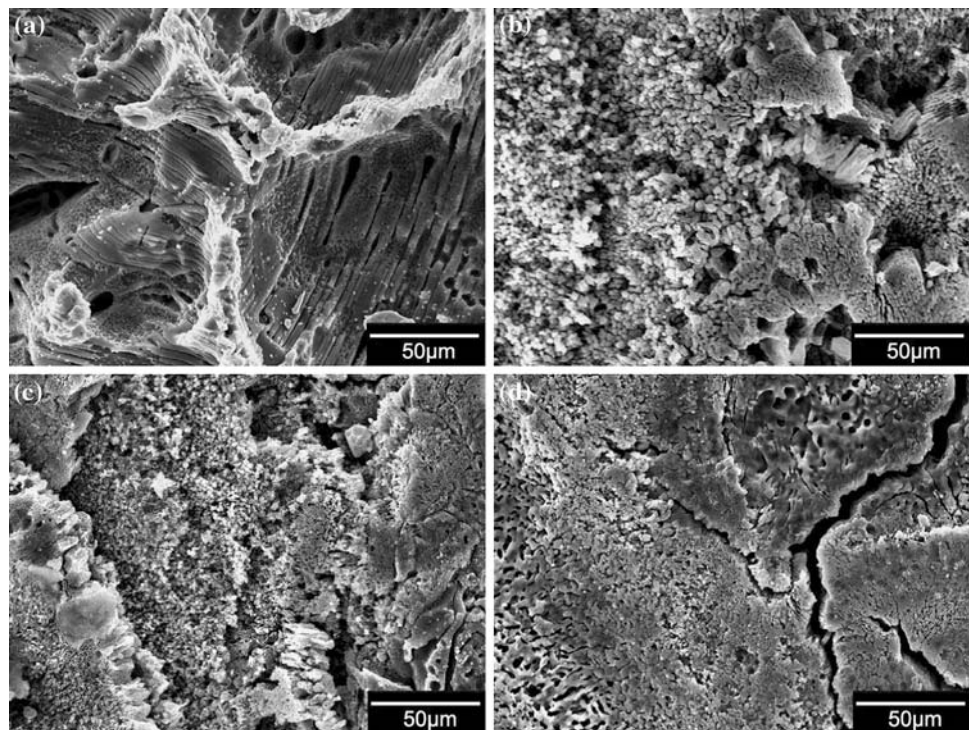


Fig. 8 Scanning electron micrographs showing corroded surfaces of **a** as-received alloy, **b** specimen A, **c** specimen B and **d** specimen C in m-SBF after exposure for 2 weeks



in specimen C were the main reasons for the increased corrosion rate.

After immersion for 2 weeks the microgalvanic corrosion at α -Mg matrix and eutectic phase accelerated in the as-received microstructure (Fig. 8a). In the laser-treated microstructure A, localized pits were found to spread

laterally along the overlapped regions to cover the whole surface, resulting in uniform corrosion (Fig. 8b). Although localized pitting corrosion in microstructure B spread, the degree of corrosion was lower than that of specimen A (Fig. 8c). Moreover, cracks in specimen C accelerated the corrosion process, as shown in Fig. 8d.

The results suggest that LSM has significant influence on corrosion behaviour of the magnesium alloy due to the refined β -Mg₁₇Al₁₂ phase. In the as-received microstructure, the bulk and lamellar β -Mg₁₇Al₁₂ phase is highly cathodic to the α -Mg phase and can thus act as an effective cathode to cause microgalvanic corrosion [4–9]. In the LSM specimens, the original microstructures were refined to the cellular/dendritic structure with the continuous network of fine β -Mg₁₇Al₁₂ phase to provide an effective barrier against corrosion. Among all the laser-treated specimens, specimen B offered the best corrosion resistance. Coarse dendritic structures in the overlapped regions (in specimen A) and cracks in the melted zones (in specimens C and D) were found to affect the corrosion resistance adversely due to too slow or too fast laser scanning rates.

3.3 Electrochemical behaviour of laser-treated microstructures

The electrochemical corrosion behaviour of LSM microstructures was compared with that of the as-received microstructure. The potentiodynamic polarization curves of all the microstructures in m-SBF are shown in Fig. 9. The values of corrosion potential (E_{corr}), Tafel slope (β_c) and the corrosion current density (i_{corr}) for each polarization curve are summarized in Table 3.

As shown in Fig. 9, corrosion potential E_{corr} for LSM microstructures was shifted to less negative values (ranging from -1.605 to -1.412 V) than that of as-received alloy (-1.725 V), indicating less corrosion susceptibility for the laser-treated microstructures. It is further noted that cathodic current i_{corr} was much lower for all laser-treated microstructures at all potentials, indicating that the laser-treated samples had lower corrosion rates. This observation

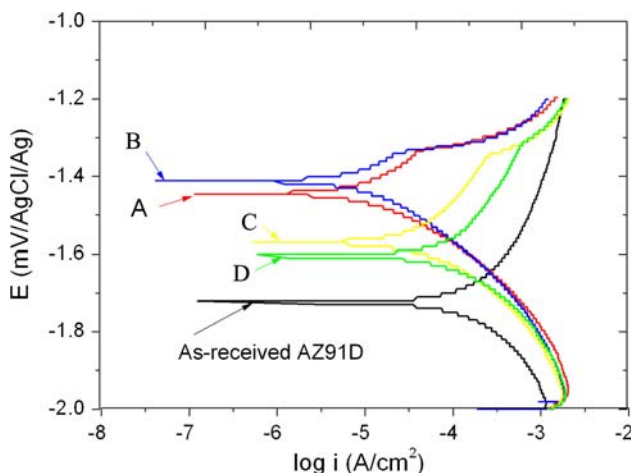


Fig. 9 Potentiodynamic polarization curves for as-received and laser-treated AZ91D alloy in m-SBF

Table 3 E_{corr} , β_c and i_{corr} values for AZ91D alloy before and after laser irradiation in m-SBF solution

Specimen ID	E_{corr} (V)	β_c (V)	i_{corr} (mA cm ⁻²)
As-received	-1.725	0.731	0.0722
A	-1.449	0.149	0.0085
B	-1.412	0.128	0.0075
C	-1.570	0.214	0.0317
D	-1.605	0.303	0.0541

is found to be in only partial agreement with the results of immersion tests (Fig. 4): after the laser treatment, the immersion corrosion rate is indeed lower for microstructures A and B but in fact higher for microstructures C and D. However, the discrepancy can be explained because the cracks in microstructures C and D are shown to accelerate corrosion during immersion tests (Figs. 7d, 8d). The β_c values are similar for microstructures A and B (0.149 and 0.128 V) or C and D (0.214 and 0.303 V), indicating the same electrochemical reactions for A and B or for C and D. The difference in β_c value between A and B on the one hand and C and D on the other may be attributed to the presence of cracks in specimens C and D.

4 Conclusions

Corrosion behaviour of AZ91D magnesium alloy after laser surface melting in the modified-simulated body fluid at 37 °C was studied using electrochemical techniques. The homogeneous microstructure led to uniform corrosion in the laser-treated specimens A and B with slow laser scanning rates due to the refined continuous network of β -Mg₁₇Al₁₂ phases and the increased average Al concentration in the laser-melted zones. However, the coarse dendrite structure in the overlapped regions along the laser tracks provided the preferential site for pitting corrosion, which resulted in poorer corrosion resistance in m-SBF for microstructure A than for microstructure B. Moreover, small cracks in the melted zones of specimens C and D with fast laser scanning rates due to high thermal stress accelerated the corrosion rate in the m-SBF. The study has clearly demonstrated that laser surface melting can be used effectively to improve corrosion resistance of biodegradable Mg alloy implants. It is hoped that the study will stimulate further research in this field.

References

1. Staiger MP, Pietak AM, Huadmai J, Dias G (2006) *Biomaterials* 9:1728
2. Liu CL, Xin YC, Tang GY, Chu PK (2007) *Mater Sci Eng A* 456:352

3. Kannan MB, Raman RKS (2008) *Biomaterials* 29:2310
4. Ambat R, Aung NN, Zhou W (2000) *J Appl Electrochem* 30:870
5. Jonsson M, Persson D, Gubner R (2007) *J Electrochem Soc* 154:C688
6. Aung NN, Zhou W (2002) *J Appl Electrochem* 32:1340
7. Ambat R, Aung NN, Zhou W (2000) *Corros Sci* 42:1437
8. Song GL, Bowles AL, St John DH (2004) *Mater Sci Eng* 366:82
9. Chang JW, Peng LM, Guo XW, Atrens A, Fu PH, Ding WJ, Wang XS (2008) *J Appl Electrochem* 38:210
10. Dubé D, Fiset M, Couture A, Nakatsugawa I (2001) *Mater Sci Eng A* 299:41
11. Liu Z, Chong PH, Skeldon P, Hilton PA, Spencer JT, Quayle B (2006) *Surf Coat Tech* 200:5520
12. Majumdar JD, Galun R, Mordike BL, Manna I (2003) *Mater Sci Eng A* 361:123
13. Oyane A, Kim HM, Furuya T, Kokubo T (2003) *J Biomed Mater Res A* 65A:191
14. Khaled MM (2003) *J Appl Electrochem* 33:820
15. Qian HX, Zhou W, Zheng HY (2008) *Surf Rev Lett* 15:475
16. Avedesian MM (1999) *Magnesium and magnesium alloys*. ASM International, Materials Park, pp 8–9
17. Zhou W, Long TZ, Mark CK (2007) *Mater Sci Technol* 23:1298
18. Huang YJ, Hu BH, Pinwill I, Zhou W, Taplin DMR (2000) *Mater Manuf Process* 15:97
19. Liu SY, Hu JD, Yang Y, Guo ZX, Wang HY (2005) *Appl Surf Sci* 252:1724
20. Pierron N, Sallamand P, Jouvard J, Cicala E, Matte S (2007) *J Phys D Appl Phys* 40:2098